GEOLOGICA CARPATHICA, AUGUST 2008, 59, 4, 295–306

An apatite-rich enclave in the High Tatra granite (Western Carpathians): petrological and geochronological study

ALEKSANDRA GAWĘDA

University of Silesia, Faculty of Earth Sciences, Będzińska st. 60, 41-200 Sosnowiec, Poland; gaweda@us.edu.pl

(Manuscript received June 25, 2007; accepted in revised form March 14, 2008)

Abstract: A mafic, coarse-grained apatite-rich enclave found in the High Tatra granite, Western Carpathians, is an ultrapotassic rock with mixed (mantle-crustal) geochemical and mineralogical signatures. A U-Pb zircon age dates the intrusion at 345 ± 5.1 Ma. Zircon cores preserve ages of 361 ± 7.6 Ma and 391 ± 4.6 Ma. The apatite-rich rock could be interpreted as a cumulate material related to common Tatra granite of comparable age (360–340 Ma). This rock, of very unusual mineralogy, is an atypical cumulate formed in rocks of granitoid composition.

Key words: Variscan, High Tatra Mts, petrology, apatite-rich cumulate, U-Pb zircon dating.

Introduction

Granites usually contain enclaves of various origins. Some are co-genetic with the host granite magma (autoliths), some are mingled magmas of more basic types, others are restite and many show no genetic links (xenoliths). All enclaves are a record of the hidden history of the granite they are enclosed in. The role of mafic magma in granite plutonism was underlined in the first half of the XXth century and is still under active investigation (Pitcher 1997; Vincenzo & Rocchi 1999; Barbarin 2005). The rock- and mineral chemistry of mafic enclaves carries information about the source, origin and evolution of the mantle contribution to the processes involved in granitoid magmatism and also about the source mantle, existing beneath the crust at the time of magma generation.

Phosphorus-rich magmatic rocks are not a common lithology in the Earth's crust. Apatite-rich lamprophyres related to peraluminous, post-collisional, 1.8 Ga granitoid intrusions occur in the Fennoscandian Shield (Konopelko et al. 1998; Eklund et al. 1998). Enclaves of biotite-apatite rocks in early Variscan (368 Ma) granites have been described from the Achala Batholith, Argentina; these are interpreted as cumulates (Dorais et al. 1997). Internal structures of granitoid rocks (*sensu lato*) resembling depositional features and interpreted as a result of accumulation of early-formed crystals (cumulates) are relatively scarce and restricted to magmas rich in water and flourine, lowering the melt viscosity (Collins et al. 2006).

In this paper, new data from an apatite-rich mafic enclave from the High Tatra granite are presented. They help to define and constrain a poorly known magmatic episode in the Variscan history of the Tatra Mountains, a part of the Central Western Carpathians.

Geological setting and sampling

The Tatra Mountains crystalline core is composed of four petrographic types of granitoids: common Tatra granodiorite-tonalite (360–340 Ma), Goryczkowa Granite (356 Ma), quartz-diorite (341 Ma) and the youngest High Tatra granite (314 Ma) (Kohút & Janák 1994; Poller et al. 2001; Gawęda et al. 2005; Burda & Klötzli 2007). All intrude a metamorphic envelope outcropping mainly in the western part of the Tatra massif (Fig. 1).

The eastern part of the Tatra Mts (High Tatra Mts) is composed of two main types of granite — a meso-Variscan S-type (340–360 Ma) and a late-Variscan hybrid I/S-type (ca. 314 Ma). The latter is rich in various types of enclaves including metasedimentary xenoliths, diorites (mafic precursors), mafic magmatic enclaves (MME), schlieren and felsic blobs (Pawlica 1918; Janák 1993; Gawęda 2005; Gawęda et al. 2005; Gawęda 2007a,b). Two basic petrographic types, biotite monzogranite and porphyritic granite, were distinguished among the High Tatra type (Gawęda 2007b). All of the granite pulses, differing in age and chemistry, form one composite, polygenetic pluton. The granite components of the pluton show VAG (Volcanic Arc Granites) geochemical characteristics and isotopic signatures that suggest continuous melting of heterogeneous metasediments during subduction of oceanic crust under the continental wedge and during which interaction with mantle melts was significant (Poller et al. 2001; Gawęda 2007b).

In the upper part of the Batyżowiecka (Batizovská) Valley, at about 1950 m on the western slopes of Gerlach Mt, a ca. 0.9 m enclave of mela-syenite with numerous K-feldspar phenocrysts was discovered in the porphyritic variety of the High Tatra granite (Figs. 1, 2a). The contact between the mafic enclave and the leucocratic porphyritic granite is sharp. The mafic enclave, the host granite, their contact zone and different petrographical types of granites (including quartz diorites) were sampled over the distance of ca. 100 m.

Analytical methods

Microscopic observations were made using a BX-60 Olympus microscope at the Faculty of Earth Sciences, University of Silesia, Sosnowiec, Poland. Microprobe analyses of minerals

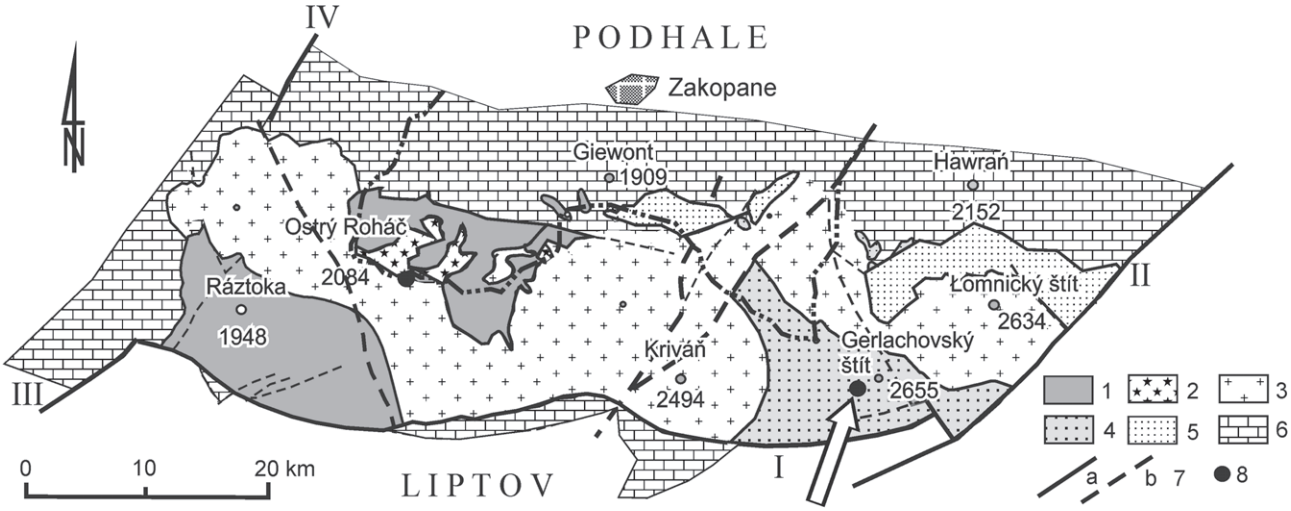

Fig. 1. Simplified geological map of the Tatra Mts massif with the location of the apatite-rich enclave sampling point (compilation after Kohút & Janák 1994; Gawęda et al. 2005). **1** — metamorphic cover, **2** — anatectic leucogranites, **3** — common Tatra granite, **4** — High Tatra granite, **5** — Goryczkowa granite, **6** — sedimentary cover, **7** — main faults: a — identified, b — assumpted, **8** — sampling point.

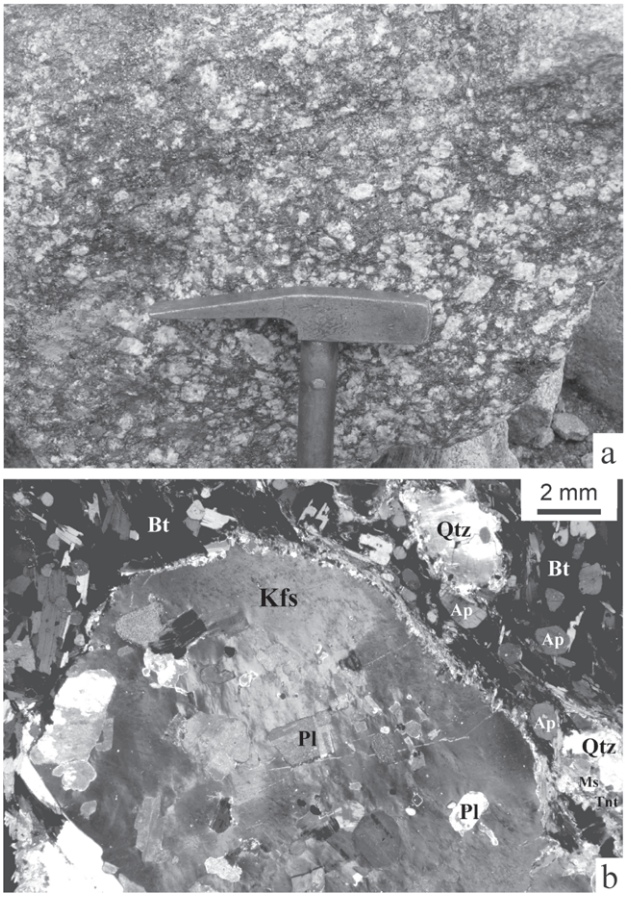

Fig. 2. Photos of apatite-rich enclave: **a** — Field photograph of the apatite-rich enclave. Geological hammer as a scale. **b** — Microphotograph of the apatite-rich enclave. Note the quartz grains, mantled by mica and titanite. Abbreviations: **Kfs** — K-feldspar, **Pl** — plagioclase, **Qtz** — quartz, **Bt** — biotite, **Ap** — apatite, **Tnt** — titanite, **Ms** — muscovite.

and BSE photographs were carried out on a CAMECA SX-100 electron microprobe in the Inter-Institution Laboratory of Microanalysis of Minerals and Synthetic Substances, Warsaw, using sets of natural and synthetic standards. Major and trace elements were analysed by XRF and ICP-MS at the ACME Analytical Laboratories, Vancouver, Canada. $^{87}Sr/^{86}Sr$ and $^{143}Nd/^{144}Nd$ isotopic ratios were measured using a VG sector 54 mass spectrometer at the Department of Geochronology, Institute of Geological Sciences, Polish Academy of Sciences, Warsaw. Values of $^{87}Sr/^{86}Sr$ were normalized to SRM 987 ($^{87}Sr/^{86}Sr = 0.710266 \pm 17$, n = 5). Values of $^{143}Nd/^{144}Nd$ were normalized to JNd-1 ($^{143}Nd/^{144}Nd = 0.512107 \pm 15$, n = 10). Zircons crystals were separated using standard techniques involving crushing, hydrofracturing, washing, Wilfley table, magnetic separator and handpicking at the Institute of Geological Sciences, Polish Academy of Sciences, Kraków. 75 zircon grains were selected for morphological studies by (SEM). Zircon and apatite morphology (SEM), their internal structures (CL) as well as 7 zircons selected for dating were imaged by SEM and CL using a FET Philips XL 30 electron microscope (15kV and 1nA) at the University of Silesia, Sosnowiec.

Zircons were dated by LA-ICP-MS at the Geochronology Laboratory, Institute of Geology, University of Vienna. Zircon $^{206}Pb/^{238}U$ and $^{207}Pb/^{206}Pb$ ages were determined using a 193 nm solid state Nd-YAG laser (NewWave UP193-SS) coupled to a multi-collector ICP-MS (Nu Instruments HR). Spot analyses were 15–25 μm in diameter. Line widths for rastering were 10–15 μm with a rastering speed of 5 μm/sec. The calculated $^{206}Pb/^{238}U$ and $^{207}Pb/^{206}Pb$ intercept values were corrected for mass discrimination from analyses of standards 91500 (Wiedenbeck et al. 1995) and Plešovice (Slama et al. 2006) measured during the analyses using a standard bracketing method. The correction involves regression of standard measurements by a quadratic function. A common Pb correction was applied to the final data using the apparent $^{207}Pb/^{206}Pb$ age and the Stacey-Kramers (1975) Pb evolution model. The

final U/Pb ages were calculated at 1 σ standard deviation using the Isoplot/Ex program — version 3.00 (Ludwig 2003).

Petrography and mineral characteristics

The porphyritic mafic enclave shows minor secondary alteration (insignificant biotite chloritization) only in the 5 mm thick contact zone. The enclosing porphyritic K-feldspar granitoid is also slightly altered near the contact. The composition of the host granitoid changes from K-feldspar syenogranite in the 1 m contact zone to the porphyritic, K-feldspar-rich monzogranite with quartz diorite enclave at about 50 m from the contact and to biotite monzogranite further out. There is no indication of cooling against the granite in the enclave and no mineralogical zoning, but the narrow (about 1 cm) fine-grained margin is noticeable inside the granite.

The medium-grained enclave (size of rock-forming minerals fall in the range of 2–8 mm) is composed of K-feldspar porphyrocrysts (~30 mm), biotite, apatite, albite, quartz and muscovite (Table 1). The accessories (< 1%) are monazite, xenotime, epidote-allanite, zircon, magnetite-ilmenite-rutile intergrowths, titanite, chlorite and calcite. The Mafic Index (MI = biotite + apatite + opaque minerals + titanite + epidote) is ca. 45 % (Gawęda 2006). A weak fabric is defined by Kfs megacrysts and biotite-apatite alignment (Fig. 2b).

The Kfs euhedral porphyrocrysts show normal zoning in BaO content from 1.86–0.91 wt. % (0.035–0.024 Ba a.p.f.u.) in cores to 0.75–0.43 wt. % (0.014–0.008 Ba a.p.f.u.) at rims (Fig. 3). Inclusions of albitic plagioclase, and falls in Ba content, emphasise the zoning of the host-feldspar (Fig. 3). The matrix plagioclase is also albite ($Ab_{93}An_5Or_2$–$Ab_{97}An_3$). Biotite (*fm* = 0.644–0.598, Ti = 0.39–0.36 a.p.f.u.) is weakly zoned with a slight drop in Ti content from core to rim (Table 2). In general, the biotite chemistry compares with that of the enclosing granite (Fig. 4). The TiO_2 content of the dispersed muscovite flakes in the range 1.3–1.7 wt. %, and *fm* in the range 0.731–0.754 (Table 2) both reflect the magmatic character of the white mica (Monier & Robert 1986). They are chemically and optically homogeneous.

Two types of apatite (0.2–2 mm Ø) were identified: Ap_1 — unzoned isometric clear apatite crystals (Figs. 2b, 5a,c; Table 3a) and prevailing Ap_2 — xenomorphic crystals with a patchy internal structure marked by differences in Fe, Y, Na and Mg contents and with inclusions of HREE-rich xenotime and zircon (Fig. 5a,b,d; Table 3b), poikiloblastically intergrown with biotite flakes.

Zircons, from 15–100 μm in size, occur as inclusions in Ap_1, in biotite and in opaque minerals. In the classification of Pupin (1980), the zircon morphologies are widely distributed with populations typical of high-temperature mantle-derived magmas (J_{1-2}), lower-temperature crustal-derived magmas (S_{6-7}–S_{16-17}) and mixtures of both (S_{21-24}, Figs. 6, 7). Zircon inclusions in apatite are of J_1 type only (Fig. 5d,e). All of the zircon crystals have cores with Zr/Hf ~43–55 and rims with Zr/Hf ~19.5–42 (Fig. 7; Table 4).

Zoned euhedral epidotes show transitions from allanite cores to REE-bearing epidote at the rims (Table 5), as is typical of magmatic epidote crystals. Secondary zoizite + titanite fringes the overgrow the REE-epidote (Table 5). Unzoned Ce-monazite crystals (Table 3b) occur as inclusions in biotite, apatite and opaque minerals, locally the decomposition of monazite and formation of REE-epidote is observed. Opaque minerals occur as aggregates of intergrown ilmenite, magnetite and rutile in varying proportions

Table 1: Modal analyses of the apatite-rich enclave and the surrounding granitoid rocks. **1** — apatite-rich enclave, **2, 3, 4** — porphyritic varieties of High Tatra type granites, **5** — quartz diorite, **6** — an example of common Tatra type granite.

Sample No.	G2-05 1	G1g-05 2	Mkn-05 3	G12g-05 4	G9d-05 5	CTG 6
Pl	6.13	51.35	38.68	37.25	46.18	60.30
Kfs	39.77	13.37	33.14	29.10	–	20.90
Qtz	4.37	18.56	16.42	19.65	6.73	16.60
Bt/Chl	30.77	9.63	6.05	7.00	41.99	1.40
Ms	4.49	2.91	4.05	4.60	0.70	0.40
Ep	0.10	–	0.96	1.00	0.65	0.25
Np+tnt	0.57	1.84	0.35	0.43	1.35	0.02
Ap	13.74	1.77	0.25	0.70	1.90	0.10
Zrn/Mnz	0.04	0.60	0.10	0.27	0.50	0.03

Table 2: Microanalyses of biotite (Bt) and muscovite (Ms) with their crystal-chemical formulas (22 O^{2-}) from the mela-syenite enclave. ***fm*** = Fe/(Fe + Mg + Mn); **c** — core, **m** — margin.

Component	Bt1c	Bt1m	Bt4c	Bt4m	Bt4r	Ms1c	Ms2c	Ms2m	Ms2r
SiO_2	35.01	34.86	34.83	34.97	35.66	44.94	44.97	45.06	44.96
TiO_2	3.26	2.48	3.33	3.12	3.08	1.63	1.70	1.31	1.62
Al_2O_3	16.84	15.72	16.84	16.93	17.02	31.51	31.48	31.80	31.37
Cr_2O_3	0.05	0.01	0.02	0.02	0.03	0.04	0.00	0.00	0.00
FeO	21.54	23.53	22.04	22.78	22.57	4.36	4.18	4.25	4.36
MgO	8.74	8.43	7.79	8.07	7.9	0.85	0.81	0.78	0.88
MnO	0.39	0.22	0.36	0.34	0.29	0.03	0.00	0.00	0.04
Na_2O	0.14	0.04	0.07	0.09	0.09	0.48	0.45	0.46	0.42
K_2O	9.4	8.88	9.17	9.22	9.28	10.37	10.42	10.30	10.37
BaO	0.00	0.04	0.06	0.02	0.19	0.12	0.04	0.14	0.06
Total	95.37	94.21	94.51	95.56	96.11	94.33	94.06	94.09	94.08
Si	5.414	5.497	5.44	5.421	5.484	6.174	6.184	6.192	6.187
Al^{IV}	2.586	2.503	2.56	2.579	2.516	1.826	1.816	1.808	1.813
Al^{VI}	0.483	0.419	0.539	0.514	0.569	3.275	3.286	3.342	3.275
Ti	0.380	0.294	0.391	0.364	0.356	0.168	0.176	0.135	0.168
Cr	0.006	0.001	0.003	0.002	0.004	0.004	0.000	0.000	0.000
Fe	2.785	3.103	2.878	2.952	2.903	0.501	0.481	0.488	0.502
Mg	2.016	1.981	1.814	1.864	1.811	0.174	0.167	0.159	0.180
Mn	0.051	0.030	0.048	0.044	0.038	0.003	0.000	0.000	0.005
Na	0.041	0.013	0.022	0.026	0.026	0.128	0.120	0.123	0.113
K	1.854	1.786	1.828	1.823	1.822	1.817	1.829	1.805	1.821
Ba	0.000	0.003	0.004	0.001	0.011	0.006	0.002	0.007	0.003
fm	0.574	0.607	0.607	0.608	0.612	0.739	0.742	0.754	0.731

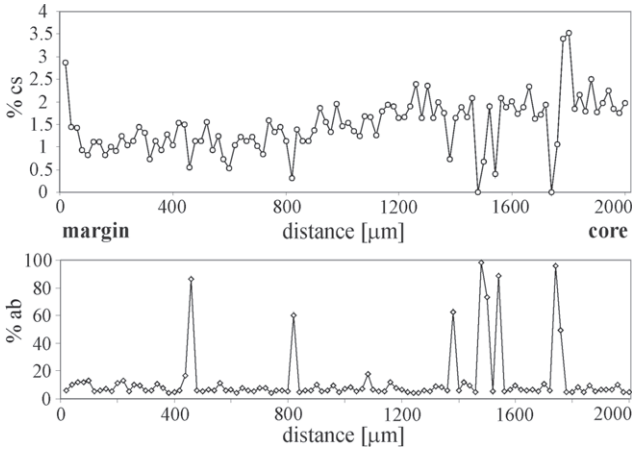

Fig. 3. Cs and Ab distribution profiles in alkali feldspar phenocryst. Scale in micrometers.

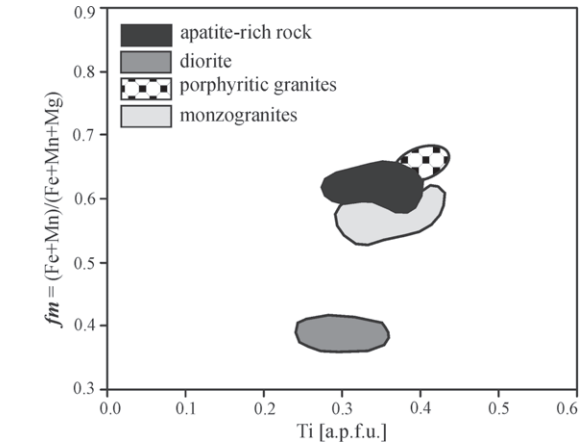

Fig. 4. Plot of biotite composition in the Ti [a.p.f.u.]/***fm*** space. For comparison biotites from porphyritic granites, monzogranites and diorites were used.

(Table 6) and suggest the decomposition of an original ulvöspinel under oxidizing conditions. The opaque crystals host tiny inclusions of calcite and are overgrown by titanite coronas. The titanite may be a product of secondary reaction between Ti-rich opaque minerals and calcite.

Whole-rock geochemistry

The rock is characterized by low SiO_2, and a very high P_2O_5 reflecting the high apatite content (Table 7). However, it is quartz (3.60) and corundum (4.34) normative (Gawęda 2006) as biotite is the main rock-forming aluminosilicate and primary muscovite is present. Petrographical observations (i.e. mantling of the quartz by micas and titanite, Fig. 2b) suggest that the quartz could have been physically wedged into the enclave.

The Fe_2O_3, TiO_2, Ba, Rb, total REE, Zr, Hf, Y contents are high and that of Sr moderate (Table 6; Fig. 8a,b,c,d). REE fractionation, dominated by HREE fractionation, is weak ($Ce_N/Yb_N = 3.16$; Table 7). The rock is characterized by a pronounced negative Eu anomaly ($Eu/Eu^* = 0.354$; Table 7; Fig. 9) and a low Sr/Sr* value ($Sr/Sr^* = Sr_N/\sqrt{[Ce_N \times Nd_N]} = 0.135$), especially when compared to the other Tatra granitoids (compare Table 7 and Gawęda 2007b). The ASI index (ASI = Al/[Ca + K + Na – 3.33P]) recalculated against the molecular P_2O_5 content equals 1.499 and the sample plots in the peraluminous field of Maniar & Piccoli (1989), while without correction to phosphorus the sample is metaluminous (ASI = 0.837). As the rock is corundum normative and magmatic micas are volumetrically important components the first value is considered here. The K_2O/Na_2O ratio is equal to 3.93, so the rock can be classified as ultrapotassic (Fig. 8e). The agpaitic index ($[K_2O + Na_2O]/Al_2O_3$[molar]) is 0.61. Sr prevails over Rb (Rb/Sr = 0.467) and Nd over Th (Nd/Th = 6.526; Fig. 8d). Zr/Hf at 32.41 is typical of most crustal rocks.

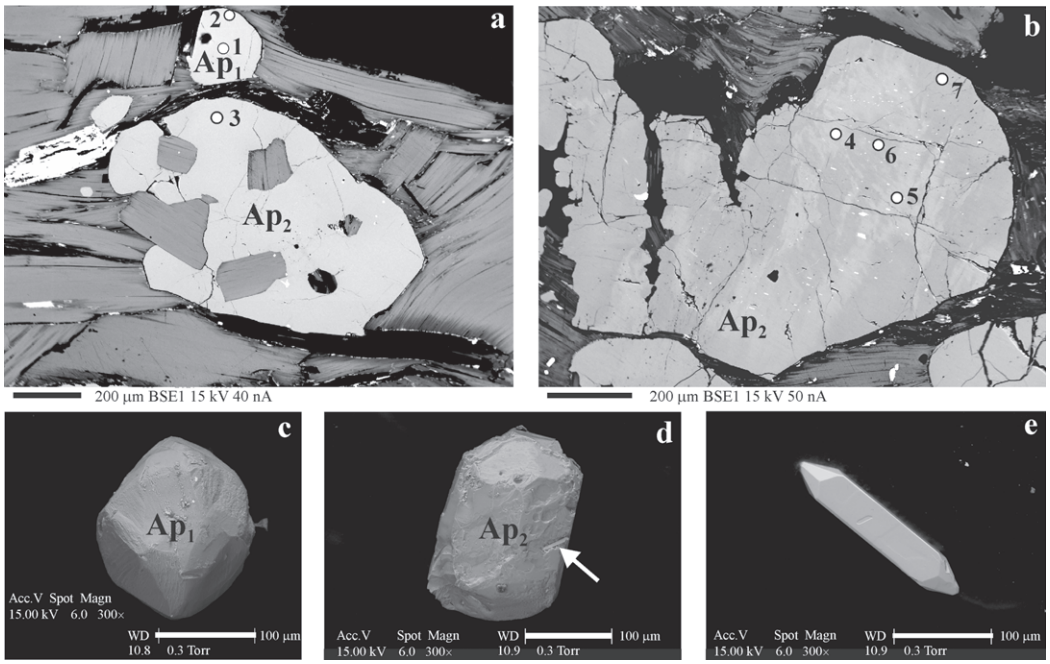

Fig. 5. Examples of SEM and BSE images of apatite and zircon. **a** — BSE image of isometric Ap_1 (analytical points of apatite 1 & 2) and xenomorphic Ap_2 (point 3), intergrown with biotite (grey). **b** — BSE image of xenomorphic Ap_2 with patchy internal structure (analytical points 4–7 adequate to analyses in Table 3a) and dissolution embayments. **c** — SEM image of Ap_1. **d** — SEM image of hipidiomorphic Ap2 with zircon inclusion (pointed by arrow). **e** — SEM image of J2 zircon crystal.

Table 3: a — Selected microanalyses of apatite. **b** — Selected xenotime and monazite microanalyses.

a

Apatite	Ap 1		Ap 2				
Analysis No.	1	2	3	4	5	6	7
P_2O_5	42.54	40.69	42.03	42.48	40.14	42.91	41.91
SiO_2	0.02	0.03	0.00	0.03	0.01	0.02	0.00
SO_2	0.00	0.04	0.02	0.01	0.05	0.03	0.05
ThO_2	0.00	0.00	0.06	0.09	0.00	0.03	0.08
Fe_2O_3	0.09	0.21	0.24	0.01	0.12	0.06	0.14
Y_2O_3	0.15	0.11	0.23	0.24	0.34	0.17	0.19
La_2O_3	0.02	0.01	0.18	0.24	0.03	0.01	0.01
Ce_2O_3	0.03	0.05	0.04	0.11	0.17	0.00	0.16
Nd_2O_3	0.13	0.10	0.00	0.01	0.15	0.00	0.16
Gd_2O_3	0.02	0.03	0.05	0.10	0.07	0.00	0.01
CaO	54.52	55.17	54.43	54.76	55.23	55.52	55.20
MnO	0.14	0.19	0.22	0.14	0.31	0.00	0.14
SrO_2	0.03	0.04	0.02	0.01	0.04	0.02	0.08
Na_2O	0.06	0.06	0.15	0.11	0.18	0.07	0.10
H_2O	0.00	0.00	0.00	0.05	0.00	0.00	0.06
F	2.71	3.63	3.25	2.12	3.90	2.43	2.12
Cl	0.03	0.04	0.04	0.02	0.04	0.01	0.02
Total	**100.41**	**100.40**	**100.73**	**100.26**	**100.78**	**101.26**	**100.43**

b

Sample	Xen 1	Xen 2	Mon 1
P_2O_5	35.13	35.01	29.60
Y_2O_3	44.19	43.12	0.00
La_2O_3	0.03	0.06	13.71
Ce_2O_3	0.03	0.15	29.09
Pr_2O_3	0.07	0.04	3.25
Nd_2O_3	0.43	0.70	12.67
Sm_2O_3	0.57	0.72	2.31
Gd_2O_3	2.66	2.85	1.51
Er_2O_3	4.09	3.73	0.12
Dy_2O_3	4.89	4.89	0.32
Ho_2O_3	1.20	0.84	0.09
Yb_2O_3	2.97	2.97	0.00
Lu_2O_3	0.71	0.73	0.00
Fe_2O_3	0.24	0.00	0.00
Tb_2O_3	0.52	0.50	0.10
SiO_2	0.15	0.16	0.20
UO_2	0.67	0.69	0.18
ThO_2	0.00	0.10	4.33
PbO	0.00	0.00	0.03
Total	**98.552**	**97.238**	**97.51**

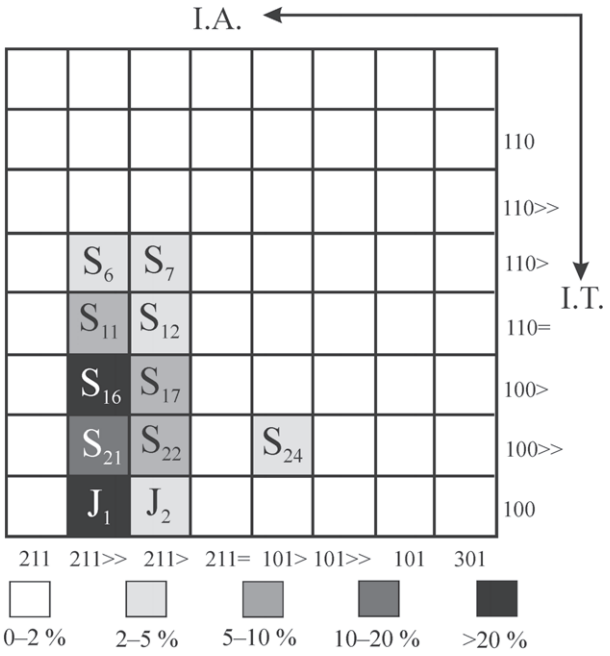

Fig. 6. The position of zircon crystals morphology on Pupin's (1980) typological diagram.

U-Pb zircon dating and isotope geochemistry

U-Pb dating of 7 zircon crystals representing both J and S morphological types (Fig. 7) reveal three generations of ages. The oldest age of 391 ± 4.6 Ma (Fig. 10a; Table 8a) was found in zircon cores and one mantle. Two zircon mantles and one core provide an age of 361 ± 7.6 Ma (Fig. 10b; Table 8b). Zircon rims, and one core with magmatic zoning, yielded the youngest age of 345 ± 5.1 Ma (Fig. 10c; Table 8c). One homogeneous inner core was dated to ca. 700 Ma and one core with oscillatory zonation to ca. 430 Ma (Table 8d).

The apatite $^{87}Sr/^{86}Sr$ can be considered to be the rock initial ratio as apatite contains little or no Rb, assuming no isotopic disturbances occurred (Tsuboi & Suzuki 2003). The apatite $^{87}Sr/^{86}Sr$ value of 0.707620, lower than whole-rock IR_{Sr}^{345} $^{87}Sr/^{86}Sr$ ratio (Table 9) suggests either a mixed mantle/crust-

Table 4: Microanalyses of zircon crystals and their crystal-chemical formulae.

Sample	Zr1(c1)	Zr1(c2)	Zr1(m)	Zr1(r)	Zr2(c)	Zr2(m)	Zr3(c1)	Zr3(c2)	Zr3(m)
SiO_2	31.98	31.91	31.13	32.15	31.92	31.98	32.15	31.27	32.18
ZrO_2	65.65	65.75	65.00	64.08	65.28	65.04	66.08	65.49	65.71
HfO_2	1.04	1.08	1.35	2.87	1.18	2.17	1.08	1.32	1.92
UO_2	0.09	0.05	0.05	0.22	0.10	0.10	0.05	0.06	0.08
Y_2O_3	0.54	0.47	0.32	0.12	0.43	0.16	0.46	0.22	0.11
Yb_2O_3	0.14	0.11	0.05	0.08	0.11	0.05	0.11	0.03	0.08
CaO	0.26	0.00	0.14	0.37	0.18	0.18	0.00	0.17	0.00
Total	**99.69**	**99.37**	**98.04**	**99.89**	**99.21**	**99.68**	**99.92**	**98.55**	**100.09**
Si	0.989	0.989	0.981	0.996	0.991	0.991	0.991	0.981	0.992
Zr	0.990	0.994	0.999	0.969	0.989	0.983	0.993	1.002	0.988
Hf	0.009	0.010	0.012	0.025	0.011	0.019	0.010	0.012	0.017
U	0.001	0.000	0.000	0.002	0.001	0.001	0.000	0.000	0.001
Y	0.009	0.008	0.005	0.002	0.007	0.003	0.008	0.004	0.002
Yb	0.001	0.001	0.001	0.001	0.001	0.001	0.001	0.000	0.001
Ca	0.009	0.000	0.005	0.012	0.006	0.006	0.000	0.006	0.000
Zr/Hf	**55.108**	**53.151**	**42.034**	**19.493**	**48.299**	**26.167**	**53.418**	**43.316**	**29.879**

Table 5: Selected microanalyses of epidotes and their crystal-chemical formulae (25 O^{2-}).

Component	Al-ep9	Al-ep10	Al-ep11	Al-ep12	Al-ep16	Al-ep13	Al-ep14	Al-ep15	Ep-r-1	Ep-r-2
	rim	mantle		core		mantle		rim	secondary	
SiO_2	33.75	32.63	33.32	32.6	31.98	32.89	33.85	34.89	37.32	37.45
TiO_2	0.1	0.19	0.12	0.17	0.22	0.13	0.06	0.11	0.01	0.04
Al_2O_3	19.35	18.06	19.08	18.06	17.65	18.69	19.98	20.36	21.66	22.09
P_2O_5	0.63	0.07	0.42	0.19	0.38	0.05	0.19	0.21	0.29	0.56
FeO	12.59	13.65	12.97	13.46	12.82	12.75	12.34	13.03	14.01	13.65
MnO	0.79	1.18	0.7	0.87	0.87	0.54	0.79	0.58	0.19	0.11
MgO	0.18	0.22	0.19	0.22	0.26	0.20	0.15	0.14	0.00	0.00
CaO	14.91	12.83	14.6	13.2	12.19	14.16	15.61	17.1	22.66	22.59
SrO	0.00	0.00	0.00	0.00	0.00	0.00	0.00	0.00	0.18	0.33
La_2O_3	2.10	3.21	2.18	3.20	3.77	3.00	1.59	1.67	0.04	0.00
Ce_2O_3	5.08	7.11	5.50	6.90	8.84	7.11	4.32	3.66	0.08	0.00
Pr_2O_3	0.62	0.81	0.61	0.71	0.97	0.75	0.53	0.41	0.03	0.00
Nd_2O_3	2.40	2.74	2.92	3.10	3.70	2.70	2.24	1.72	0.04	0.08
Sm_2O_3	0.65	0.54	0.66	0.59	0.74	0.64	0.61	0.32	0.02	0.04
Gd_2O_3	0.44	0.48	0.48	0.50	0.43	0.40	0.72	0.50	0.07	0.14
ThO_2	0.01	0.19	0.21	0.14	0.10	0.00	0.14	0.08	0.02	0.12
V_2O_3	0.00	0.00	0.00	0.03	0.01	0.01	0.00	0.01	0.03	0.03
Total	**93.60**	**93.91**	**93.96**	**93.94**	**94.93**	**94.02**	**93.12**	**94.79**	**96.66**	**97.22**
Si	6.169	6.166	6.144	6.15	6.089	6.151	6.180	6.193	6.219	6.180
Ti	0.014	0.027	0.016	0.024	0.032	0.018	0.008	0.015	0.002	0.005
Al	4.168	4.022	4.146	4.016	3.960	4.119	4.300	4.259	4.255	4.296
Fe	1.924	2.156	2.000	2.124	2.041	1.995	1.883	1.935	1.952	1.884
Mn	0.122	0.190	0.109	0.138	0.140	0.085	0.123	0.087	0.027	0.015
Mg	0.050	0.063	0.051	0.061	0.075	0.055	0.041	0.037	0.000	0.001
Ca	2.920	2.596	2.884	2.669	2.487	2.836	3.053	3.252	4.046	3.993
Sr	0.000	0.000	0.000	0.000	0.000	0.000	0.000	0.000	0.018	0.032
La	0.142	0.223	0.148	0.222	0.264	0.207	0.107	0.109	0.002	0.000
Ce	0.340	0.492	0.371	0.476	0.616	0.487	0.289	0.238	0.005	0.000
Pr	0.041	0.056	0.041	0.049	0.067	0.051	0.035	0.027	0.002	0.000
Nd	0.157	0.185	0.192	0.209	0.252	0.180	0.146	0.109	0.002	0.005
Sm	0.041	0.035	0.042	0.038	0.049	0.041	0.038	0.019	0.001	0.002
Gd	0.027	0.030	0.029	0.031	0.027	0.025	0.044	0.030	0.004	0.007
Th	0.001	0.008	0.009	0.006	0.004	0.000	0.006	0.003	0.001	0.004

Table 6: Selected microanalyses of magnetite (**sp**) and ilmenite (**Il**) and their crystal-chemical formulae (for 4 O^{2-} and 3 O^{2-} respectively).

Sample	sp1	Ilm1	sp2	Ilm2	sp3	Ilm3	sp4
FeO	31.06	41.35	30.71	40.87	31.3	40.85	30.73
Fe_2O_3	66.37	4.04	55.6	3.77	66.52	4.49	67.8
MnO	0.05	3.87	0.64	4.65	0.00	4.18	0.07
MgO	0.00	0.06	0.00	0.06	0.04	0.06	0.00
Cr_2O_3	0.07	0.00	0.05	0.00	0.07	0.00	0.06
V_2O_5	0.81	0.00	0.41	0.00	0.47	0.00	0.43
Nb_2O_5	0.24	0.01	0.15	0.00	0.21	0.00	0.06
TiO_2	1.81	50.46	11.32	50.81	1.38	50.24	1.03
Total	**100.41**	**99.78**	**98.88**	**100.16**	**99.99**	**99.82**	**100.18**
Fe^{+2}	0.986	0.875	0.975	0.862	0.994	0.865	0.975
Fe^{+3}	1.896	0.077	1.588	0.072	1.900	0.086	1.937
Mn^{+2}	0.002	0.083	0.019	0.100	0.000	0.090	0.002
Mg^{+2}	0.000	0.002	0.000	0.002	0.002	0.002	0.000
Cr^{+3}	0.002	0.000	0.002	0.000	0.002	0.000	0.002
V^{+5}	0.020	0.000	0.010	0.000	0.012	0.000	0.011
Nb^{+5}	0.005	0.001	0.003	0.000	0.004	0.000	0.001
Ti^{+4}	0.052	0.960	0.323	0.964	0.039	0.957	0.029

Notice: sp2 and Ilm2 are not in equilibrium

al origin for the rock or, perhaps, some disturbance of a primary value. A three point errorchron based on apatite, Kfs and the host whole rock suggests an age of 312 ± 530 Ma ($IR_{Sr}^{312} = 0.70740$). The rock is characterized by an IR_{Nd}^{345} value of 0.511901, ε_{Nd}^{345} and crustal residence age $T_{DM} = 1.341$ (Table 9). It is worth mentioning that both the Sr and Nd isotopic characteristics of the apatite rock resemble those found in most Variscan granitoid rocks (Kohút et al. 1999).

Discussion

The origin of the apatite-rich rock and its systematic position

Low SiO_2 and high CaO contents reflect the high apatite content. The high Al_2O_3 content and peraluminous character of the rock are due to the high contents of biotite and muscovite; both minerals are peraluminous–biotite because of its significant siderophyllite component. The modal and chemi-

Table 7: Whole-rock analyses of major and trace elements in the apatite-rich enclave (G2-05), the selected granitoids (G1g-05, Mkn-05, G12g-05) and quartz-diorite enclave (G9d-05). T_{Zr} — temperature calculated according to Watson & Harrison (1983) procedure. CTG — an example of common Tatra granite.

Sample No.	G2-05	G1g-05	Mkn-05	G12g-05	G9d-05	CTG
SiO_2	48.89	62.9	64.74	66.66	61.07	75.62
TiO_2	1.23	0.65	0.52	0.58	0.77	0.11
Al_2O_3	16.21	18.87	17.78	17.04	17.91	13.48
Fe_2O_3	7.98	3.23	3.19	3.61	5.89	0.67
MnO	0.11	0.02	0.04	0.05	0.09	0.01
MgO	2.7	1.92	1.23	1.13	2.73	0.13
CaO	7.21	1.67	1.48	2.41	3.33	0.94
Na_2O	1.67	4.71	3.88	4.49	4.31	3.07
K_2O	6.57	3.56	5.14	2.39	2.33	5.10
P_2O_5	5.08	0.25	0.32	0.28	0.36	0.15
LOI	2.00	2.30	1.60	1.50	1.3	0.90
C(tot)	0.04	0.15	0.02	0.05	0.01	0.03
S(tot)	0.01	0.01	0.01	0.01	0.01	0.01
Total	99.7	100.24	99.95	100.2	100.11	100.18
ASI	1.499	1.301	1.228	1.199	0.821	0.957
Sr	384.3	319.5	445.4	499.6	735.2	370.1
Ba	2538.5	1093.7	2421.9	705.7	681.9	1477.4
Rb	179.6	91.9	110.4	73.2	107.5	131.4
Th	25.1	15.9	9.3	9.9	2	0.4
U	8.7	1.7	1.8	2.6	19.3	1.0
Cr	20.5	20.6	23	103	47.9	48.0
V	125	59	48	126	115	9.0
Zr	440.8	205.8	159.1	143.8	122	41.7
Hf	13.6	6.0	4.2	3.9	3.6	1.5
Y	401.1	16.8	20	26.1	22	5.1
Nb	19.7	8.5	8.8	11.3	8.6	2.7
Ta	1.0	0.5	0.5	0.8	0.6	0.3
La	105.70	49.70	14.20	39.90	17	4.40
Ce	266.60	104.60	29.40	84.90	65.6	9.20
Pr	36.90	11.98	3.36	10.37	129.6	1.12
Nd	163.80	42.80	12.20	41.00	14.13	4.10
Sm	54.10	8.50	3.00	9.40	50.6	1.20
Eu	6.78	1.69	0.69	1.56	8.6	0.59
Gd	63.48	5.89	2.98	7.78	1.58	0.94
Tb	12.23	0.91	0.66	1.35	6.01	0.18
Dy	72.06	3.99	4.58	7.65	0.84	0.99
Ho	14.07	0.56	0.96	1.49	4.24	0.18
Er	35.49	1.36	3.00	4.29	0.72	0.47
Tm	4.64	0.20	0.44	0.64	1.91	0.08
Yb	23.27	1.15	2.49	3.70	0.3	0.39
Lu	3.00	0.19	0.37	0.57	1.62	0.09
Eu/Eu*	0.354	0.730	0.657	0.600	0.672	1.698
$(Ce/Yb)_N$	3.157	25.061	12.950	11.655	22.042	6.500
T_{Zr} [°C]	**752**	**822**	**797**	**801**	**754**	**695**

cal composition of the apatite-rich rock cannot, in any case, represent liquid, so it cannot be interpreted as a microgranular enclave. There are a number of ways in which the enclave rock may have originated. It may be (a) restite, (b) cumulate, (c) recrystallized metasediment or (d) magmatic rock unrelated to the host granite. The lack of a negative Ce-anomaly and the high REE, Ba, Zr, Y and Hf contents (Table 8) tell against it being a P-rich metasediment (see Dorais et al. 1997). Moreover, there is no field and mineralogical evidence that the enclave was a metasomatized country rock. The negative Eu anomaly and the high LILE content are atypical of restite. On the other hand, a magmatic origin is supported by the internal structures of minerals (zonation).

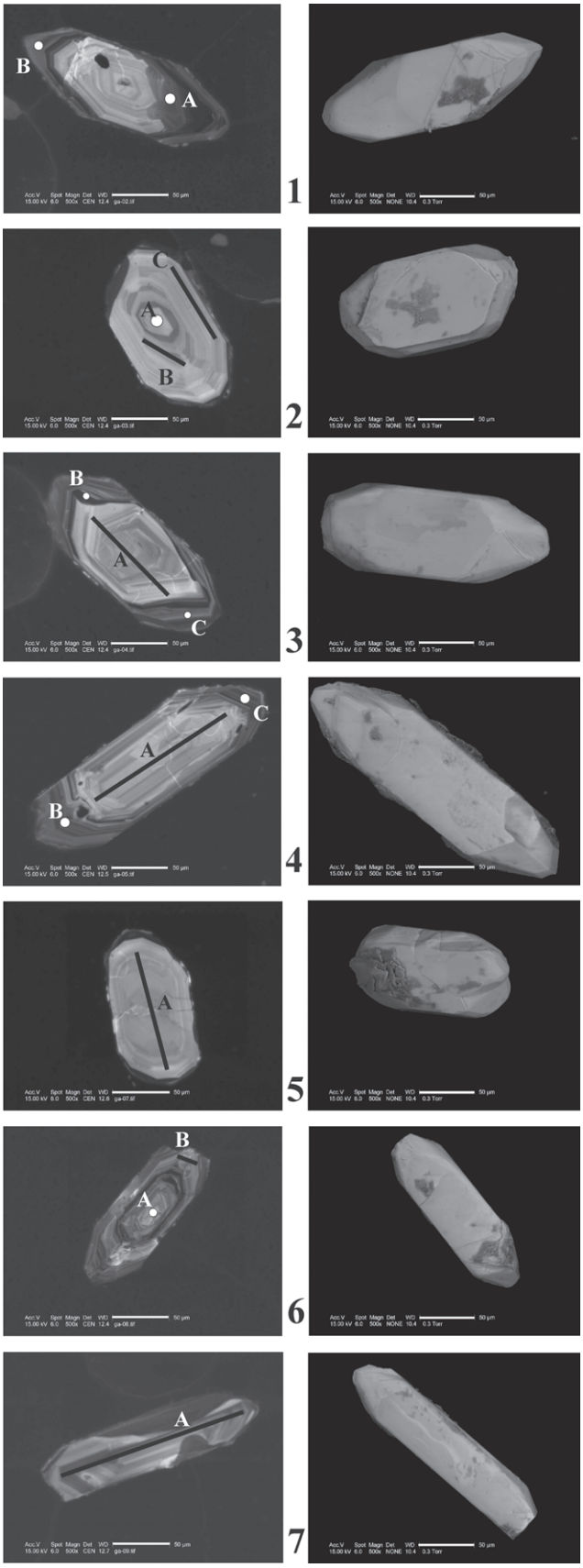

Fig. 7. CL and SEM images of zircon crystals used for U-Pb dating. Analytical lines and points marked not to scale.

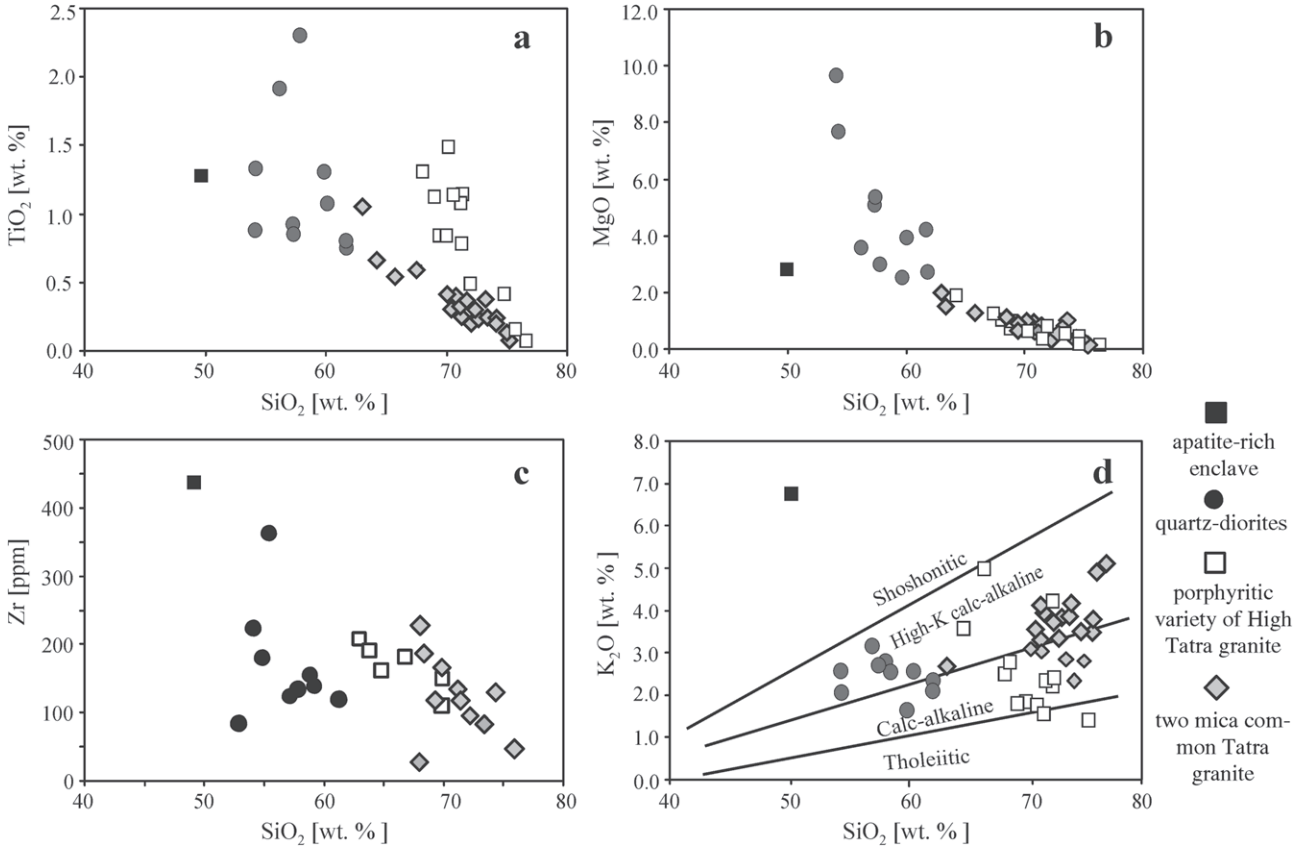

Fig. 8. Selected Harker diagrams of the apatite-rich enclave, diorites and host High Tatra granites.

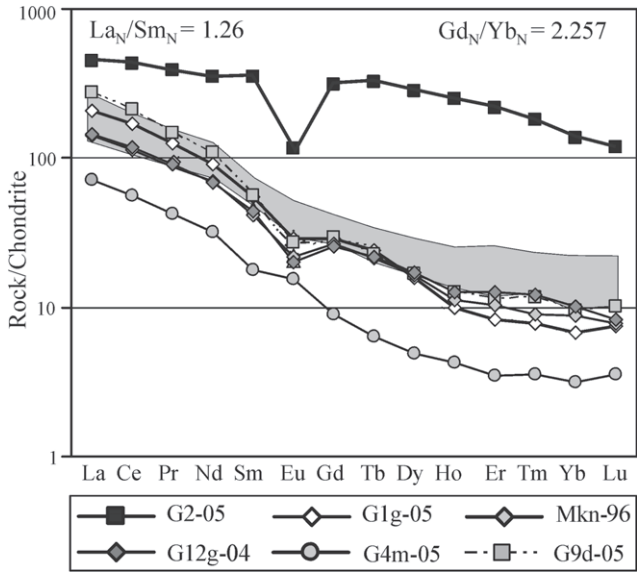

Fig. 9. Chondrite-normalized (C1 chondrite, after Sun & Mc Donough 1989) REE patterns of the apatite-rich enclave, host granitoids and metapelitic xenoliths. Symbols explanations: **G2-05** — apatite-rich enclave, **G1g-05** — porphyritic granite from the contact, **Mkn-96** and **G12g-04** — porphyritic granites 9 m and 20 m from the contact, **G4m-05** — monzogranite from the Upper Batizovská Valley, **G9d-05** — quartz diorite from the Upper Batizovská Valley. Grey area cover the quartz-diorites C1-normalized REE values.

The high REE content, the flat chondrite-normalized pattern and the high HFSE content combined with low SiO_2 (Table 8) could point to a mantle derivation or to its origin as a cumulate. The undepleted HREE rule out residual garnet in the source. The source similar to MORB can also be excluded as partial melting would give HREE-depleted, fractionated magmas. The prevalence of Nd over Th (Fig. 8d) is also indicative for mantle-derived rocks. The strong negative Eu anomaly, and the high Cr/Ni (4.1), low Zr and Nb contents suggest a mantle fractionate or a related cumulate rock. A low Sr/Sr* value indicates relative Sr depletion analogous to that of Eu; both suggest feldspar fractionation with a plagioclase-rich residue.

The low transitional-metal content, the high LILE concentration, and the high La/Nb (22.64) open the possibility of the rock being a crustal melt. The prevalence of Fe over Mg is also atypical of mantle derivatives as is the high Al_2O_3 content (Table 7). The extreme P_2O_5, enrichment, high P_2O_5/TiO_2 and high LILE content have been noted as typical of low fraction lithospheric mantle melts (Backer & Wyllie 1992). With only one sample, any fractional pattern calculations are impossible.

As a magmatic rock, the apatite-rich enclave can be classified as quartz mela-syenite (IUGS classification) or apatite-rich mela-syenodiorite (TAS classification — Le Maitre et al. 1989). The rock plots in the shoshonitic field in contrast to the calc-alkaline and high-K calc-alkaline host granitoid suites (Fig. 8d).

Table 8: LA ICP-MS isotope data from zircon grains from apatite-rich enclave. For the location of the analytical points (sample numbers) see Fig. 7. U and Pb concentrations were not determined because sample weighing was not possible.

a

Sample No.	Atomic ratios						Rho	Apparent age (Ma)			
	$^{207}Pb/^{235}U$	1 σ	$^{206}Pb/^{238}U$	1 σ	$^{207}Pb/^{206}Pb$	1 σ		$^{207}Pb/^{235}U$	1 σ	$^{206}Pb/^{238}U$	1 σ
1.A	0.47281	0.04051	0.06771	0.00584	0.05271	0.00021	0.4950	393	15	422	11
2.B	0.44719	0.03834	0.06210	0.00284	0.05160	0.00113	0.2665	374	5	388	7
3.A	0.44935	0.13408	0.06441	0.01959	0.05328	0.00055	0.5096	377	9	402	11
4.A	0.46563	0.08492	0.06267	0.00086	0.05600	0.00082	0.0373	389	1	392	2
5.A	0.47748	0.04180	0.06074	0.00281	0.05577	0.00114	0.2641	396	4	380	5

b

Sample No.	Atomic ratios						Rho	Apparent age (Ma)			
	$^{207}Pb/^{235}U$	1 σ	$^{206}Pb/^{238}U$	1 σ	$^{207}Pb/^{206}Pb$	1 σ		$^{207}Pb/^{235}U$	1 σ	$^{206}Pb/^{238}U$	1 σ
1.B	0.40820	0.09204	0.05910	0.01130	0.0532	0.0006	0.4264	348	13	368	11
3.B	0.41864	0.01803	0.06052	0.00353	0.0522	0.0003	0.6770	356	14	379	10
7.A	0.43492	0.02152	0.05815	0.00170	0.0547	0.0002	0.2946	367	4	364	5

c

Sample No.	Atomic ratios						Rho	Apparent age (Ma)			
	$^{207}Pb/^{235}U$	1 σ	$^{206}Pb/^{238}U$	1 σ	$^{207}Pb/^{206}Pb$	1 σ		$^{207}Pb/^{235}U$	1 σ	$^{206}Pb/^{238}U$	1 σ
2.C	0.43526	0.03516	0.05490	0.00517	0.0570	0.0008	0.583	367	8	345	10
3.C	0.37542	0.06985	0.05553	0.01236	0.0491	0.0007	0.598	331	9	349	11
4.B	0.40431	0.02764	0.05582	0.00375	0.0544	0.0005	0.491	345	8	350	11
4.C	0.40357	0.05170	0.05773	0.00729	0.0529	0.0003	0.493	344	9	362	10
6.B	0.40324	0.00760	0.05664	0.00143	0.0520	0.0002	0.668	344	13	355	9

d

Sample No.	Atomic ratios						Rho	Apparent age (Ma)			
	$^{207}Pb/^{235}U$	1 σ	$^{206}Pb/^{238}U$	1 σ	$^{207}Pb/^{206}Pb$	1 σ		$^{207}Pb/^{235}U$	1 σ	$^{206}Pb/^{238}U$	1 σ
2.A	0.99380	0.14755	0.11797	0.01220	0.06376	0.0005	0.3482	701	5	719	6
6.A	0.52587	0.18324	0.07036	0.00912	0.05419	0.0007	0.1860	429	4	438	3

Table 9: Isotopic analyses of apatite-rich rock, its mineral separates and comparable rock-types. **G2-05** — apatite rich enclave, **G9d-05** — quartz-diorite enclave, **G12g-04** — porphyritic variety of High Tatra type granite, **CTG** — an example of common Tatra granite. Errors are given in 2 σ.

Isotope parameter	G2-05	G9d-05	G12g-04	CTG
Rb [ppm]	179.6	107	73.2	111.3
Sr [ppm]	384.3	735.2	499.6	370.1
$^{87}Sr/^{86}Sr$ WR	0.713624±11	0.707074±11	0.709021	0.711642
$^{87}Rb/^{86}Sr$ WR	1.352949	0.421059	0.423972	0.886077
$^{87}Sr/^{86}Sr$ Ap	0.707620±11	–	–	–
$^{87}Sr/^{86}Sr$ Kfs	0.710478±21	–	–	–
$^{87}Rb/^{86}Sr$ Kfs	0.680109	–	–	–
IR_{Sr}^{345}	0.706980	0.705006	0.707126	0.707038
Sm [ppm]	54.1	8.6	6.7	1.2
Nd [ppm]	163.8	50.6	32.1	4.1
$^{143}Nd/^{144}Nd$ WR	0.512463±5	0.512472±8	0.512360±13	0.512410±28
$^{147}Sm/^{144}Nd$	0.199678	0.102753	0.126188	0.176948
$^{143}Nd/^{144}Nd$ Ap	0.512618±15	–	–	–
IR_{Nd}^{345}	0.511901	0.512103	0.511944	0.511894
ε_{Nd}^{345}	–3.548	0.902	–2.318	–3.580
T_{DM} [Ga]	1.341	0.989	1.242	1.353

Time of the apatite-rich rock formation

U-Pb zircon dating provides different Variscan ages. Zircons crystallized early enough to be included in biotite and apatite. In the context of the geological history of the Tatra Mts massif, cores yielding 391 Ma and some older exceptions possibly reflect the metamorphic events and/or partial melting episodes in the Tatra Massif (Fig. 10a,b; Burda 2006, 2007; Gawęda 2007b). The concordant age of 361 Ma is in accordance with both the common Tatra granite age (Poller et al. 2000) and the age of Western Carpathians Variscan granite magmatism (365 Ma; Kohút et al. 1999) as well as with the partial melting processes in the Western Tatra Mts (Burda 2006, 2007). The concordant age from the zircon rims (345 Ma; Fig. 10c) compares closely with a U-Pb zircon age for quartz diorites (341 Ma; Poller et al. 2001), a WR Rb-Sr isochron age for Western Tatra pegmatites (ca. 345 Ma; Gawęda 1995) and a K-Ar age for shear-zone muscovite (ca. 343 Ma; Deditius 2004).

The Rb-Sr three-point errochron age of ca. 312 Ma, and a zircon lower intercept U-Pb age of 314 ± 4 Ma for the High Tatra granite intrusion (Poller et al. 2001), are consistent with 300–330 Ma Ar-Ar age of Variscan uplift of the High Tatra Mts (Janák 1994) and 298–318 K-Ar ages of shearing (Deditius 2004) and, presumably, final cooling of the Tatra crystalline massif.

Temperature and pressure determinations

The thermometer of Watson & Harrison (1983), based on rock Zr content, applied for the apatite-rich rock, provided a temperature of 752 °C without correction for Ca in apatite, while after correction the calculated temperature increased to 890 °C. For the other Tatra granitoid rocks the temperature intervals are as follows: 822–797 °C for the Kfs-rich pophyritic granites, 806–736 °C for the biotite monzogranites and

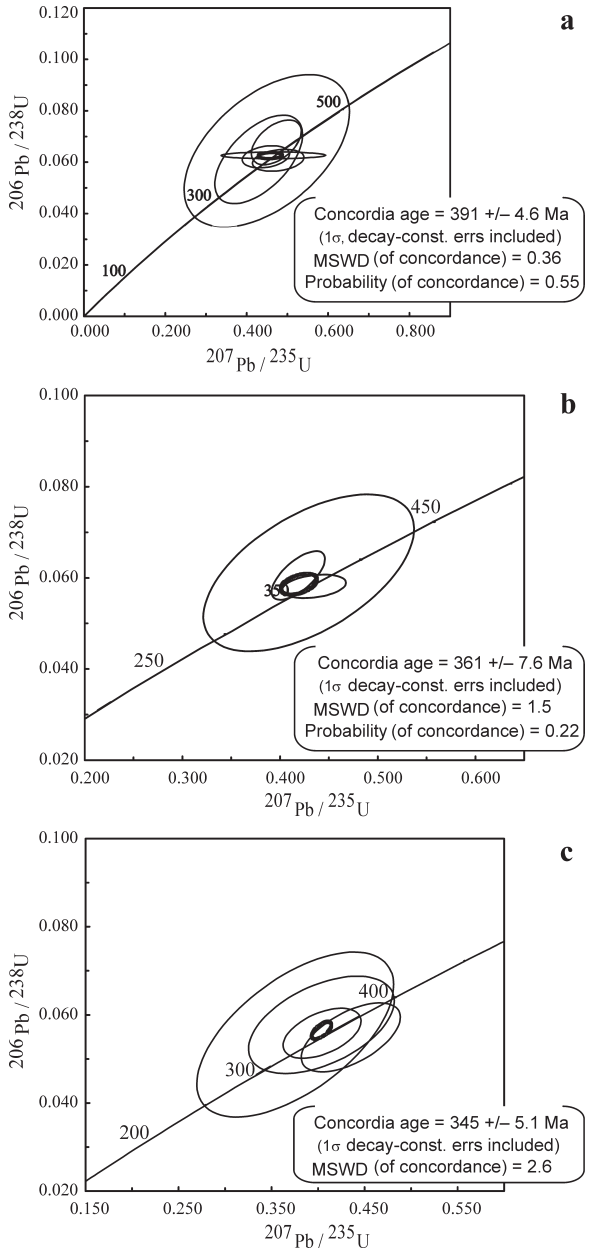

Fig. 10. $^{206}Pb/^{238}U$ *versus* $^{207}Pb/^{235}U$ Concordia plots for the analysed zircon grains from apatite-rich enclave. **1** — concordia plot for 391 ± 4.6 Ma zircon cores, **2** — concordia plot for 361 ± 7.6 Ma zircon core and mantles, **3** — concordia plot for 345 ± 5.1 Ma zircon rims.

822–753 °C for the quartz diorites (Gawęda 2007b), and the correction for Ca in apatite is insignificant. As the rock chemical and mineralogical composition cannot be interpreted in terms of liquid, both temperatures are of doubtful meaning.

For the apatite-rich rock, calculation of the Mt-Ilm exsolution (Spencer & Lindsley 1981) gave a temperature of exsolution in the range 680–668 °C in a growing oxygen fugacity regime ($\log_{10}fO_2 = -16$). The latter temperature range is similar to earlier determinations for the High Tatra granitoids (Grabowski & Gawęda 1999).

The flat REE profile of the enclave constrains the depth of melt origin. High-pressure (22–32 kbar) melts in equilibrium with an eclogitic residue show highly fractionated HREE depletion with low Yb contents, whereas low-pressure (~8 kbar) melts with no residual garnet show weakly fractionated REE patterns (Luais & Hawkesworth 1994) similar to that of the enclave (Fig. 9). Magmatic zoned epidote with allanitic cores (Table 4), that crystallized after biotite but before quartz and K-feldspar, suggests a pressure >6–8 kbar. The temperature of the crystal mush for the given P did not exceed 740–775 °C for $H_2O > 9$ wt. % (Schmidt & Poli 2004). Assuming the high concentration of volatiles in the magma, suggested by the lack of "dry" minerals and the presence of biotite as the predominant mafic mineral, the higher temperature limit can be approved (Schmidt & Poli 2004), covering temperatures revealed by Mt-Ilm geothermometer, conspicuously consistent with zircon thermometry. Biotite chemical zoning, although weak, means growing oxygen fugacity as Ti is incorporated into oxides.

The presence of allanite-epidote also suggests the changes in Ca activity in the melt as monazite crystallization typifies low-Ca activity conditions, and allanite presence, high Ca activity (Broska et al. 2000). Possibly, early apatite (Ap_1) crystallization lowered the Ca activity enabling monazite crystallization, and Ap_2 maintained it so. Afterwards, the remaining Ca was used for allanite formation during more oxidizing conditions while plagioclase is almost pure albite (Petrík & Broska 1994).

The zoned K-feldspars, and changes in barium content, can be interpreted in terms of magma mixing and/or changing parent-magma temperatures, water contents, crystallization of additional minerals, etc. (Long & Luth 1986; Słaby et al. 2002). As barium diffusivity in alkali feldspars is very low, zoning is usually a primary feature. No features such as perthite coarsening identify the influence of post-magmatic fluids in the subsolidus stage (see Brown & Parsons 1989). The perturbations observed in the analysed profile (Fig. 3) may reflect changes in the crystallization path due, in the main, to falling water contents — favouring crystallization of the plagioclase now trapped as inclusions in the Kf megacrysts. Increased Ba in Kf near each albite inclusion could reflect increasing water contents in the magma and/or new mantle magma input. After the Ba decrease to the margin, the Kf megacryst rims show renewed Ba-enrichment (up to 0.029 a.p.f.u., 1.58 wt. % BaO — see Fig. 3). This may represent crystallization from a residuum rich in water, and in Ba.

The calculated temperature interval of 700–800 °C is the crystallization temperature of most of the rock-forming silicates in the apatite-rich enclave as oxygen fugacity increased. The Mt-Ilm geothermometry (680–668 °C) could reflect cooling on intrusion of the crystal mush and the decomposition of primary opaque mineral phases. The assumed pressure (6–8 kbar) is at the higher end for the hybrid quartz diorite magma range (4–6 kbar; Gawęda et al. 2005). The enclave crystallization and cooling temperatures compare with those of the surrounding granites (Gawęda 2007b). Thus, the cooling history of the hosting granite may have been the key influence.

Speculative model of the apatite-rich magma formation

The apatite, which is the rock-forming mineral in the rock in question, is a carrier of both F and P, elements significantly

lowering the magma viscosity. Fluorine and phosphorus enrichment could allow formation of a cumulate, typical rather of basic and alkaline rocks (Collins et al. 2006). Here the term cumulate is used without defining the specific process of its formation. That could be both crystal sorting caused by gravity or during magma flow in the stress field. The last possibility is supported by the oriented fabric of the apatite-rich rock and the presence of tectosilicates (micas).

The hybrid character of the apatite rock suggests some similarities with quartz diorites of roughly the same age (ca. 341 Ma; compare data and discussion in Gawęda et al. 2005). However, the differences in ε_{Nd}^{345} and in T_{DM} values point out the different source of both rock-types (compare: Table 9 and Poller et al. 2001). The processes like cumulate formation or fractional crystallization could not change the isotopic characteristics of the magma. On the selected Harker diagrams (Fig. 8a,b,c) diffuse trends links the apatite-rich enclave rather to common Tatra granites then to quartz diorites. However, it must be noted that most of the quartz-diorites occur as xenoliths in younger (ca. 314 Ma) High Tatra granites and were subjected to secondary recrystallization (see Gawęda et al. 2005). Moreover, the linear trends typically produced by mixing/mingling and fractional crystallization processes could be easily destroyed if cumulates were produced early and more evolved liquids were mingled/mixed with the magmas differing in origin and chemistry (Collins et al. 2006).

Both the IR_{Sr}^{345} and the apatite $^{87}Sr/^{86}Sr$ ratios (0.706980 and 0.707620 adequately) could suggest at least mixed (I/S) origin (Table 9). As the apatite $^{87}Sr/^{86}Sr$ ratio is higher then IR_{Sr}^{345} either system disturbance or the "foreign" character of apatite in the rock can be suggested. The whole-rock Rb-Sr isotopic system may have been easily disturbed by a younger episode or may not be representative of the real whole-rock value if the enclave size (and consequently the sample) is small. Another possibility is the assumption that during filter pressing of the cumulate material the squeezed melt was mixed and isotopically equilibrated with more mafic magma. The presence of a large amount of interstitial liquid might influence the equilibration between the enclave and the host magma (Elburg 1996). In fact, apatite Ap_2 crystals, showing deep dissolution embayments and irregular internal zoning (Fig. 5a,b), could be interpreted in terms of magma mixing regime (Słaby & Martin 2008). The incoherence between the U-Pb zircon dating (last marked episode at 345 Ma) and the Rb-Sr errorchrone point out that more then one process affected the isotope system and diffusion played an important role (Elburg 1996).

The measured apatite $^{143}Nd/^{144}Nd$ ratio is lower than that in the whole-rock sample, but higher than IR_{Nd}^{345} (Table 9). Because of the slow diffusion the LREE are thought to be less sensitive to secondary processes than Rb-Sr system (Pin et al. 1990). The calculated ε_{Nd}^{345} value of –3.548 (Table 9) would imply a crustal provenance for the enclave. As both ε_{Nd}^{345} and the calculated T_{DM} model age of the enclave (1.341 Ga, Table 9) are similar to those calculated for common Tatra granites (sample CGT, Table 9, Gawęda, in print), and also fall in the interval stated for typical West Carpathian Variscan granites (Kohút et al. 1999) it is possible that the enclave material was in a crustal environment for a long time or it is genetically linked with it.

Assuming the genetic link between the common Tatra granite (360–340 Ma) and apatite-rich cumulate the U-Pb age of 361 Ma, found in selected zircon grains (one core with magmatic zonation and 2 mantles) together with 345 Ma zircon rims, can mirror one prolonged magmatic process. Such a long time span for a magmatic activity marks either the magma convection in the chamber and/or the replenishment by the mafic magma pulses, forming together the prolonged magma crystallization and formation of the hybrid features. Such a conclusion is consistent with the presence of two MME types, representing two mingling episodes (Gawęda, in print). The presence of the cumulate enclave, showing features of both crustal- and mantle-derived magma influence, shed new light on the origin and history of meso-Variscan granitoid magmatism, till now assumed to be purely S-type.

Concluding remarks

1. Chemical and mineralogical signatures suggest that the apatite-rich enclave has a hybrid character with similarities to the ca. 360–340 Ma common Tatra granite. It can reasonably be interpreted as the cumulate fraction, formed by the crystal accumulation, possibly during magma flow.

2. The present enclave mineralogy is a result of mostly magmatic processes (magma mixing/mingling), and changes in water content, calcium activity and oxygen fugacity, usually occurring during magma mixing.

3. The P-T history of the rock was partly overprinted by the younger High Tatra granite. Petrographical and geochemical data suggest that the temperature reached 740–775 °C 8 kbar at the base of the crystal-mush layer.

4. The ca. 361–345 Ma hybrid apatite-rich rock is a unique feature of the geology of the Tatra Mts massif that spans a history of the meso-Variscan magmatism.

Acknowledgments: R. Piwkowski and E. Lichota, Tatra guides, are thanked for help during climbing, field work and sample transportation. Dr P. Dzierżanowski and Mrs. L. Jeżak helped with microprobing and E. Teper with zircon imaging. Dr J. Burda did the zircon dating in Vienna University. Prof. U. Klötzli provided the Lam-Tool computer program for U-Pb data correction and plotting. Prof. J.A. Winchester (Keele University, GB) and Dr P.S. Kennan (University College Dublin, Ireland) are thanked for English corrections and for discussions during the investigation. The work gained substantially from advice from Prof. B. Bonin, Prof. E. Słaby and from reviewer's comments by Dr I. Broska, Dr I. Petrík and Prof. R. Kryża. Polish Ministry of Sciences and Education Grant No. 2 PO4D 05629 founded the research.

References

Backer M.B. & Wyllie P.J. 1992: High-presure apatite solubility in carbonate liquids: implications for mantle metasomatism. *Geochim. Cosmochim. Acta* 56, 3409–3422.

Barbarin B. 2005: Mafic magmatic enclaves and mafic rocks associated with some granitoids of the central Sierra Nevada batholith, California: nature, origin, and relations with the

host. *Lithos* 80, 155–177.

Beard J.S. 2008: Crystal-melt separation and the development of isotopic heterogeneities in hybrid magmas. *J. Petrology* 49, 5, 1027–1041.

Broska I., Petrík I. & Williams C.T. 2000: Coexisting monazite and allanite in peraluminous granitoids of the Tribeč Mountains, Western Carpathians. *Amer. Mineralogist* 85, 22–32.

Brown W.L. & Parsons I. 1989: Alkali feldspars: ordering rates, phase transformations and behaviour diagrams for igneous rocks. *Mineral. Mag*. 53, 25–42.

Burda J. 2006: U-Pb zircon age of partial melting in metapelites from the Western Tatra Mts. *Miner. Pol., Spec. Pap.* 29, 111–114.

Burda J. 2007: U-Pb zircon age of leucogranite formation ion the crystalline basement of the Western Tatra Mts. *Miner. Pol., Spec. Pap.* 31, 85–88.

Burda J. & Klötzli U. 2007: LA-MC-ICP-MS U-Pb zircon geochronology of the Goryczkowa type granite — Tatra Mts., Poland. *Miner. Pol., Spec. Pap.* 31, 89–92.

Collins W.J., Wiebe R.A., Heally B. & Richards S.W. 2006: Replenishment, crystal accumulation and floor aggradation in the megacrystic Kameruka Suite, Australia. *J. Petrology* 47, 11, 2073–2104.

Deditius A. 2004: Characteristic and isotopic age of the muscovite blasthesis from the mylonitic zones in the crystalline rocks of the Western Tatra Mountains. *University of Silesia Publishing House*, *Geology*, 16, 121–152 (in Polish, English abstract).

Dorais M.J., Lira R., Chen Y. & Tingey D. 1997: Origin of biotite-apatite-rich enclaves, Achala batholiths, Argentina. *Contr. Mineral. Petrology* 130, 31–46.

Eklund O., Konopelko D., Rutanen H., Fröjdö S. & Shebanov A.D. 1998: 1.8 Ga Svekofenian post-collisional shoshonitic magmatism in the Fennoscandian shield. *Lithos* 45, 87–108.

Elburg M.A. 1996: Evidence of isotopic equilibration between microgranitoid enclaves and host granodiorite, Warburton Granodiorite, Lachlan Fold Belt, Australia. *Lithos* 38, 1–22.

Gawęda A. 1995: Geochemistry and Rb/Sr isochron age of pegmatites from the Western Tatra Mts. (S-Poland). *Geol. Carpathica* 46, 2, 95–99.

Gawęda A. 2005: P-T metamorphic evolution preserved in metapelitic xenoliths from the High Tatra granite. *Miner. Soc. Pol., Spec. Pap.* 25, 286–290.

Gawęda A. 2006: Apatite-rich rock from the High Tatra Granite, Western Carpathians. *Miner. Soc. Pol., Spec. Pap.* 29, 127–130.

Gawęda A. 2007a: Mafic microgranular enclaves in the High Tatra Granite — preliminary report. *Miner. Pol., Spec. Pap.* 31, 111–114.

Gaweda A. 2007b: Variscan granitoid magmatism in the Tatra Mountains — the history of subduction and continental collision. *Granitoids in Poland – AM Monographs* No. 1, 319–332.

Gawęda A., Doniecki T., Burda J. & Kohút M. 2005: The petrogenesis of quartz-diorites from the Tatra Mountains (Central Western Carpathians): An example of magma hybridisation. *Neu. Jb. Mineral. Petrology* 191, 1, 95–109.

Grabowski J. & Gawęda A. 1999: Preliminary paleomagnetic study of the High Tatra granites, Central Western Carpathians, Poland. *Geol. Quart.* 43, 3, 263–276.

Janák M. 1993: Calc-silicate metamorphic rocks of the High Tatra crystalline basement. *Miner. Slovaca* 25, 177–182 (in Slovak).

Janák M. 1994: Variscan uplift of the crystalline basement, Tatra Mts., Central Western Carpathians: evidence from $^{40}Ar/^{39}Ar$ laser probe dating of biotite and P-T-t paths. *Geol. Carpathica* 45, 5, 293–300.

Kohút M. & Janák M. 1994: Granitoids of the Tatra Mts., Western Carpathians: Field relations and petrogenetic implications. *Geol. Carpathica* 45, 5, 301–311.

Kohút M., Kovach V.P., Kotov A.B., Salnikova E.B. & Savatenkov V.M. 1999: Sr and Nd isotope geochemistry of Hercynian granitic rocks from the Western Carpathians — implications for granite genesis and crustal evolution. *Geol. Carpathica* 50, 6, 477–487.

Konopelko D., Eklund O. & Ivanikov V. 1998: 1.8 Ga phosphorus-rich lamprophyre-granitoid complex in the Fennoscandian shield: parental magmas and fractionation paths. *Acta Univ. Carolinae, Geol.* 42, 1, 51–54.

Le Maitre R.W., Bateman P., Dudek A., Keller J., Lameyre Le Bas M.J., Sabine P.A., Schmid R., Sorensen H., Streckeisen A., Woolley A.R. & Zenettin B. 1989: A classification of igneous rocks and glossary of terms. *Blackwell*, Oxford, 1–193.

Long P.E. & Luth W.C. 1986: Origin of K-feldspar megacrysts in granitic rocks: implication for the partitioning model for barium. *Amer. Mineralogist* 71, 367–375.

Luais B. & Hawkesworth C.J. 1994: The generation of the continental crust: an integrated study of the crust forming processes in the Archean Zimbabwe. *J. Petrology* 28, 921–953.

Ludwig K.R. 2003: Isoplot/Ex version 3.00. A geochronological toolkit for Microsoft Excel. *Berkeley Geochronology Center., Spec. Publ*. 4.

Monier G. & Robert J.-L. 1986: Titanium in muscovites from two-mica granites: substitution mechanism and partition with coexisting biotites. *Neu. Jb. Mineral. Abh.* 153, 147–161.

Pawlica W. 1918: Garłuchowskie calc-silicate rocks. *Rozprawy Wydziału Matematyczno-Przyrodniczego* 13, 107–130 (in Polish).

Petrík I. & Broska I. 1994: Petrology of two granite types from the Tribeč Mountains, Western Carpathians: an example of allanite (+magnetite) versus monazite dichotomy. *Geol. J.* 29, 59–78.

Pitcher W.S. 1997: The nature and origin of granite. 2nd edition. *Chapman & Hall,* London–New York, 1–387.

Poller U., Todt W., Kohút M. & Janák M. 2001: Nd, Sr, Pb isotope study of the Western Carpathians: implications for the Paleozoic evolution. *Schweiz. Mineral. Petrogr. Mitt*. 81, 159–174.

Pupin J.P. 1980: Zircon and granite petrology. *Contr. Mineral. Petrology* 73, 207–220.

Schmidt M.W. & Poli S. 2004: Magmatic epidote. *Rev. Mineral. Geochem., MSA*, 56, 399–430.

Slama J., Kosler J., Schaltegger U., Tubrett M. & Gutjahr M. 2006: New natural zircon standard for laser ablation ICP-MS U-Pb geochronology. Abstract WP05, *Winter Conference on Plasma Spectrochemistry*, Tucson, 187–188.

Słaby E. & Martin H. 2008: Mafic and felsic magma interaction in granites: the Hercynian Karkonosze pluton (Sudetes, Bohemian Massif). *J. Petrology* 49, 2, 353–391.

Słaby E., Galbarczyk-Gąsiorowska L. & Baszkiewicz A. 2002: Mantled alkali-feldspar megacrysts from the marginal part of the Karkonosze granitoid massif (SW-Poland). *Acta Geol. Pol.* 52, 4, 501–519.

Spencer K.J. & Lindsley D.H. 1981: A solution model for coexisting iron-titanium oxides. *Amer. Mineralogist* 66, 1189–1201.

Stacey J.S. & Kramers J.D. 1975: Approximation of terrestrial lead isotope evolution by a two-stage model. *Earth Planet. Sci. Lett.* 26, 207–221.

Tsuboi M. & Suzuki K. 2003: Heterogeneity of initial $^{87}Sr/^{86}Sr$ ratios within a single pluton: evidence from apatite strontium isotopic study. *Chem. Geol.* 199, 189–197.

Vincenzo G.D. & Rocchi S. 1999: Origin and interaction of mafic and felsic magmas in evolving late orogenic setting: the Early Paleozoic Terra Nova Intrusive Complex, Antarctica. *Contr. Mineral. Petrology* 137, 15–35.

Watson T.M. & Harrison E.B. 1983: Zircon saturation revisited: temperature and composition effects in a variety of crustal magma types. *Earth Planet. Sci. Lett.* 64, 295–304.

Wiedenbeck M., Alle P., Corfu F., Griffin W.L., Meier M., Oberli F., von Quadt A., Roddick J.C. & Spiegel W. 1995: Three natural zircon standards for U-Th-Pb, Lu-Hf, trace element and REE analyses. *Geost. Newsletter*, 19, 1–23.